A dispensable role of oligodendrocyte-derived laminin-α5 in brain homeostasis and intracerebral hemorrhage

Minkyung Kang[1,*], **Abhijit Nirwane**[1,*], **Jingsong Ruan**[1,*] ,
Aravinthan Adithan[1], **Marsilla Gray**[1], **Lingling Xu**[1,2] and
Yao Yao[1]

Abstract
Laminin, a major component of the basal lamina in the CNS, is also expressed in oligodendrocytes (OLs). However, the function of OL-derived laminin remains largely unknown. Here, we performed loss-of-function studies using two OL-specific laminin-α5 conditional knockout mouse lines. Both mutants were grossly normal and displayed intact blood-brain barrier (BBB) integrity. In a mouse model of intracerebral hemorrhage (ICH), control mice and both mutants exhibited comparable hematoma size and neurological dysfunction. In addition, similar levels of hemoglobin and IgG leakage were detected in the mutant brains compared to the controls, indicating comparable BBB damage. Consistent with this finding, subsequent studies revealed no differences in tight junction protein (TJP) and caveolin-1 expression among control and knockout mice, suggesting that neither paracellular nor transcellular mechanism was affected in the mutants. Furthermore, compared to the controls, both mutant lines showed comparable oligodendrocyte number, oligodendrocyte proliferation rate, MBP/MAG levels, and SMI-32 expression, highlighting a minimal role of OL-derived laminin-α5 in OL biology. Together, these findings highlight a dispensable role of OL-derived laminin-α5 in both brain homeostasis and ICH pathogenesis.

Keywords
Intracerebral hemorrhage, blood-brain barrier, laminin, oligodendrocyte, myelination

Introduction

Stroke, as the 5th leading cause of death in the United States,[1] leads to enormous socio-economic burden. Depending on the type of injury to blood vessels (rupture or ischemia), stroke is broadly categorized into hemorrhagic and ischemic stroke. Hemorrhagic stroke is the deadliest type of stroke, and unfortunately no effective treatments are available currently. One key pathology of intracerebral hemorrhage (ICH), a major type of hemorrhagic stroke, is blood-brain barrier (BBB) disruption. It has been shown that BBB disruption induces secondary brain injury and correlates with ICH outcomes.[2–7] In addition, mounting studies report white matter injury and oligodendrocyte (OL) damage after ICH.[8–10]

OLs are the only myelinating cells in the CNS. They are differentiated from oligodendrocyte precursor cells (OPCs), which are highly proliferative in adult brains. OPCs differentiate into pre-myelinating OLs (pre-OLs), which subsequently mature into myelinating mature-OLs. Mature-OLs wrap axons with lipid-rich myelin sheaths, enabling efficient signal conduction.

[1]Department of Molecular Pharmacology and Physiology, Morsani College of Medicine, University of South Florida, Tampa, FL, USA
[2]Current Address: Department of Pediatrics, Emory University School of Medicine, Atlanta, GA, USA

*These authors contributed equally to this work.

Corresponding author:
Yao Yao, Department of Molecular Pharmacology and Physiology, Morsani College of Medicine, University of South Florida, 12901 Bruce B. Downs Blvd., MDC 8, Tampa, FL 33612, USA.
Email: yao7@usf.edu

Previous in vitro studies have shown that the differentiation and maturation of OLs are delicately regulated by laminin,[11] an extracellular matrix (ECM) protein.

Laminin is a heterotrimeric protein with one α chain, one β chain, and one γ chain. In mammals, five α, four β, and three γ chains have been identified, which generate many laminin isoforms.[11,12] Interestingly, different cells make distinct laminin isoforms. In the CNS, all laminin isoforms are found exclusively at the basal lamina (BL) of the BBB, suggesting important roles of laminin in BBB regulation. Using various laminin conditional knockout mouse lines, we have systemically investigated the functions of endothelium-, pericyte-, and astrocyte-derived laminin in BBB integrity. We have shown that distinct vascular cell-derived laminin contributes to BBB maintenance to different extents.[13–18] In addition, endothelial laminin-α5 repairs BBB integrity and hemorrhagic brain injury,[15] whereas mural cell-derived laminin-α5 exacerbates BBB damage and ischemia-reperfusion injury.[16]

Whether non-vascular cells make laminin and the functional significance of non-vascular cell-derived laminin remain largely unknown. Recent RNA-sequencing studies revealed various laminin chains in OLs.[19–21] In addition, a secretome analysis reported laminin-α5 expression in pre-myelinating OLs.[22] To investigate the function of OL-derived laminin-α5, we generated two conditional knockout mouse lines. Both mutants were grossly normal under homeostatic conditions and exhibited comparable changes as the controls after ICH. These results suggest dispensable roles of OL-derived laminin-α5 in BBB maintenance/repair, OL biology, and ICH outcomes.

Materials and methods

Animals

The Laminin-α5$^{flox/flox}$ mice (a generous gift from Dr. Jeffrey Miner) were generated in a previous study.[23] Olig2-Cre$^+$ (Jax: 025567) and Sox10-Cre$^+$ (Jax: 025807) mice were obtained from the Jackson Laboratory. To generate the α5-OKO^{Olig2} (Laminin-α5$^{flox/flox}$;Olig2-Cre$^+$) and α5-OKO^{Sox10} (Laminin-α5$^{flox/flox}$;Sox10-Cre$^+$) mice, Laminin-α5$^{flox/flox}$ mice were crossed with Olig2-Cre$^+$ and Sox10-Cre$^+$ mice, respectively. Wildtype littermates were used as controls for α5-OKO^{Olig2} and α5-OKO^{Sox10} mice. All mice were maintained on a C57Bl6 background and housed in the animal facility of the University of South Florida and provided with ad libitum access to food and water. In this study, mice at the age of 4∼6 months were used. The experimental protocols and procedures of this study were approved by the Institutional Animal Care and Use Committee at the University of South Florida and were conducted in accordance with the National Institutes of Health's Guide for the Care and Use of Laboratory Animals. We adhered to the Animal Research: Reporting In Vivo Experiments (ARRIVE) guidelines for reporting experiments.

Intracerebral hemorrhage (ICH)

Mice of each genotype were randomly divided into sham and ICH groups. For those in ICH group, ICH was induced by intracerebral injection of collagenase as described in our previous publications.[15,24] Briefly, mice were anesthetized using isoflurane (3–4%, Isoflurane USP, Piramal Pharma Limited, India) and secured in a stereotaxic apparatus (RWD Life Science Co., Limited, China). To maintain moisture, artificial eye ointment (CLC Medica, Ontario, Canada) was applied to the eyes during surgery. A cranial burr hole with a diameter of 1 mm was drilled at a position 2.4 mm lateral and 0.2 mm posterior to the bregma. Next, collagenase (type VII-S; Sigma, St. Louis, USA; 0.15 U in 0.48 μl saline) was injected into the striatum (depth: 3.7 mm) using a Hamilton syringe over 5 minutes. Following the injection, the needle was left in place for 10 minutes to prevent reflux and then slowly withdrawn. Mice injected with an equivalent volume of saline served as sham controls. To prevent postsurgical dehydration, 0.5 ml of normal saline was administered intraperitoneally.

Body weight loss and behavioral tests

Body weight loss was calculated daily up to 7 days post injury (dpi). Neurological function was assessed by performing the modified neurological severity score (mNSS) test,[15,24] which scores on six different parameters (body symmetry, gait, climbing ability, circling behavior, front limb symmetry, and compulsory circling) on a scale of 0 to 4 with a maximum cumulative score of 24. Higher scores reflect more severe neurological deficits. Sensorimotor function was assessed by performing the corner test as described previously.[25] Ten trials were performed for each mouse and the total number of turns to the ipsilateral side was counted. Animals with less than 20% or more than 80% ipsilateral turns before injury were excluded. Data are presented as the percentage of turns to the ipsilateral side. To ensure unbiased assessments, the investigators conducting the evaluations were blinded to the genotypes of the mice.

Sample processing

At different time points after the injury, mice were transcardially perfused with PBS followed by 4%

paraformaldehyde (PFA). The brains were then post-fixed in 4% PFA overnight at 4 °C and immersed in 30% sucrose solution for 24 hours. Next, eight 20 μm-thick serial sections were collected using a Cryostat (Micro HM 550, Thermo Scientific). The sections were stored at −80°C until analyses.

Hematoma volume

The size of hematoma was quantified as hematoma volume (mm^3) and hematoma volume percentage (%) using serial sections as described previously.[26,27] Briefly, brain sections were subjected to cresyl violet staining and imaged using a Nikon Eclipse Ti microscope. The areas of the contralateral hemisphere (Ci), ipsilateral hemisphere (Ii), and ipsilateral non-injured region (Ni) were determined using the Image J software (NIH). Hematoma volume (mm^3) was calculated using hematoma area and the distance between serial sections. Hematoma volume (%) was calculated as:

$$\text{Hematoma volume } (\%) = \left(\frac{\sum_i \left(\left(\frac{I_i - N_i}{I_i} \right) C_i \right)}{2 \sum_i C_i} \right) \times 100$$

In situ hybridization (RNAscope)

In situ hybridization was conducted using the RNAscope multiplex fluorescent reagent kit V2 (Advanced Cell Diagnostics, 323100), according to the manufacturer's instructions. *Lama5* (494911-C2), *Olig2* (447091-C3), *and Sox10* (435931-C3) specific probes and Opal^{TM} dyes were used to visualize mRNA expression. Sections were imaged using a Nikon Eclipse Ti microscope or LSM710 confocal microscope, and analyzed using NIH ImageJ software.

Immunohistochemistry

Immunohistochemical analyses were performed according to standard protocols. Briefly, brain sections were fixed in 4% PFA for 15 minutes at room temperature and washed in PBS for 3 times. Next, the sections were blocked in blocking buffer (5% normal donkey serum in PBS + 1% BSA + 0.3% Triton X-100) for 2 hours at room temperature, followed by incubation with primary antibodies overnight at 4 °C. The following primary antibodies were used in this study: rabbit anti-Ki67 (1:200, GeneTex: GTX16667), rabbit anti-Hemoglobin (1:500, Cloud-Clone, PAB409Mu01), donkey anti-mouse IgG (1:400, Invitrogen A21203), rabbit anti-ZO-1 (1:400, ThermoFisher 61-7300), mouse anti-Claudin-5 (1:200, Invitrogen 35-2500), rabbit anti-Caveolin-1 (1:400, Cell Signaling 323AS),

mouse anti-Olig2 (1:200, Millipore MABN50), goat anti-PDGFRα (1:400, R&D Systems AF1062), rat anti-MBP (1:200, Biorad MCA409S), rabbit anti-MAG (1:300, Cell Signaling, 9043S), mouse anti-SMI-32 (1:300, BioLegend, 801701), and goat anti-podocalyxin (1:400, R&D Systems AF1556). After extensive washes in PBS, the sections were incubated with appropriate secondary antibodies for 2 hours at room temperature. Then, the sections were washed in PBS for 3 times and mounted in Fluoromount-G with DAPI. For Olig2 staining, the M.O.M.^{TM} Kit (Vector Laboratories, Inc., FMK-2201) was used. Images were taken using a Nikon Eclipse Ti microscope or LSM710 confocal microscope. Image processing was performed using ImageJ and Adobe Photoshop.

Image analyses

Brain angioarchitecture analyses were performed using the open source "Angiotool" software (National Cancer Institute, USA) as described previously.[28] Briefly, brain sections were subjected to podocalyxin staining. Vessel length, defined as the sum of Euclidean distances between the pixels of all vessels; vessel density, defined as the percentage of area occupied by vessels inside the explant area; and branching index, defined as the number of vessel junctions per unit area, were calculated in both cortex and striatum. Thresholding was applied to remove small particles so that only actual vessels were quantified. For quantifications, at least three random fields from each section, 8 serial sections per brain, and 4 mice were used. Data in α5-OKO^{Olig2} and α5-OKO^{Sox10} mice were normalized to that in controls.

TJP levels were quantified as TJP coverage and contact over blood vessels. Briefly, brain sections were subjected to ZO-1/Claudin-5 and podocalyxin staining. The area and length of ZO-1, Claudin-5, and podocalyxin signals were determined using the Angiotool software. ZO-1/Claudin-5 coverage was quantified as the percentage (%) of ZO-1/Claudin-5-positive area over podocalyxin-positive vascular area. Similarly, ZO-1/Claudin-5 contact was quantified as the percentage (%) of ZO-1/Claudin-5-positive length over podocalyxin-positive vascular length. Caveolin-1 coverage and contact over blood vessels were quantified similarly as described above. In addition, caveolin-1 intensity was also determined using ImageJ (NIH). For BBB permeability assay, the mean fluorescence intensity and area of hemoglobin and IgG were quantified. For MBP, MAG, and SMI-32 staining, fluorescent signal areas were selected by thresholding using ImageJ (NIH), and mean fluorescence intensity within the selected areas was quantified. OL number was determined by counting Olig2$^+$ cells. OL proliferation was

quantified as the percentage of Olig2$^+$ Ki67$^+$ cells over total Olig2$^+$ cells. For quantifications, at least two random fields from each section, 4 serial sections per brain, and 4–5 animals were used. All analyses were performed on z-projection images.

Statistical analyses

All statistical analyses were performed using the GraphPad Prism 9 software. Data were tested for normality using Shapiro-Wilk test. For normally distributed measurements, unpaired Student's t-test was used to determine statistical significance between two groups, and one-way analysis of variance (ANOVA) followed by Tukey post-hoc test was used for three or more groups. For comparisons involving two variables (different time points and different genotypes), two-way ANOVA followed by Tukey post-hoc test was performed. For measurements that were not normally distributed, the non-parametric Mann-Whitney U test (two groups) and the Kruskal-Wallis test (three or more groups) were used. Significance was set at $p < 0.05$. Data were presented as mean $\pm$ SD. N represents number of biological replicates.

Results

Laminin-α5 is ablated in OLs in both α5-OKO^{Olig2} and α5-OKO^{Sox10} mice

To study the function of OL-derived laminin-α5, we generated two conditional knockout mouse lines: α5-OKO^{Olig2} and α5-OKO^{Sox10}. We first validated the knockout efficiency with in-situ hybridization using striatal tissues (Figure S1(a)). In control mice, strong *Lama5* expression was detected in *Olig2$^+$* (Figure S1(b)) and *Sox10$^+$* (Figure S1(c)) cells, confirming laminin-α5 expression in OL lineage cells. In sharp contrast, no *Olig2$^+$Lama5$^+$* and *Sox10$^+$Lama5$^+$* cells were found in α5-OKO^{Olig2} (Figure S1(b)) and α5-OKO^{Sox10} (Figure S1(c)) mice, respectively. These results indicate that *Lama5* is successfully abrogated in OL lineage cells in α5-OKO^{Olig2} and α5-OKO^{Sox10} mice.

The α5-OKO^{Olig2} and α5-OKO^{Sox10} mice are grossly normal under homeostatic conditions

The α5-OKO^{Olig2} and α5-OKO^{Sox10} mice were indistinguishable from their wildtype littermates and showed comparable behaviors as the controls. To determine if loss of laminin-α5 in OLs affects vascular structure in the brain, we performed angioarchitectural analyses using podocalyxin staining (Figure 1(a) and (b)). Comparable vessel length (Figure 1(c)), vessel density (Figure 1(d)), and branching index (Figure 1(e)) were

found in α5-OKO^{Olig2}, α5-OKO^{Sox10}, and control brains, suggesting that loss of OL-derived laminin-α5 does not affect the structure of cerebral vasculature.

Hematoma volume is not changed in α5-OKO^{Olig2} and α5-OKO^{Sox10} mice after ICH

We further asked if loss of laminin-α5 in OLs affects brain injury in an ICH model. Control mice exhibited a hematoma volume of 13.64 ± 4.94 mm^3 at 3 dpi, which decreased to 5.87 ± 1.20 mm^3 at 7 dpi. (Figure 2(a) and (b)). Similar hematoma size was observed in both mutant mice after ICH. Specifically, α5-OKO^{Olig2} mice displayed a hematoma volume of 13.92 ± 5.11 mm^3 and 4.79 ± 1.86 mm^3 at 3 dpi and 7 dpi, respectively (Figure 2(a) and (b)). α5-OKO^{Sox10} mice showed a hematoma volume of 16.23 ± 4.94 mm^3 and 4.70 ± 1.64 mm^3 at 3 dpi and 7 dpi, respectively (Figure 2(a) and (b)). Similarly, quantification of hematoma volume percentage revealed comparable changes among control ($8.44 \pm 2.83\%$ and $4.83 \pm 0.80\%$ at 3 dpi and 7 dpi, respectively), α5-OKO^{Olig2} ($8.68 \pm 2.38\%$ and $3.94 \pm 1.08\%$ at 3 dpi and 7 dpi, respectively), and α5-OKO^{Sox10} ($9.87 \pm 1.48\%$ and $4.89 \pm 1.88\%$ at 3 dpi and 7 dpi, respectively) mice after ICH (Figure 2(a) and (c)). These results suggest a minimal role of OL-derived laminin-α5 in hemorrhagic brain injury.

Neurological function is unaffected in α5-OKO^{Olig2} and α5-OKO^{Sox10} mice after ICH

Both α5-OKO^{Olig2} and α5-OKO^{Sox10} mice exhibited similar body weight loss as the controls after ICH (Figure 2(d)). To further characterize neurological dysfunction in the mutants, we performed mNSS test. Control mice showed significantly increased mNSS scores after ICH (Figure 2(e)), indicating successful induction of ICH. Like the controls, both mutant lines demonstrated higher mNSS scores after ICH (Figure 2(e)). Comparison among genotypes, however, revealed no statistical significance (Figure 2(e)). Similarly, increased turns to the ipsilateral side were observed in control and mutant mice after ICH (Figure 2(f)), again indicating successful induction of ICH. Comparison among groups, however, revealed no statistical significance (Figure 2(f)). These results suggest a negligible role of OL-derived laminin-α5 in neurological function after ICH. Given that sex affects stroke outcomes,[29–31] we further analyzed these results in male and female mice separately but failed to detect any sex-specific effects (Figure S2). Together, these findings highlight a dispensable role of OL-derived laminin-α5 in ICH outcomes.

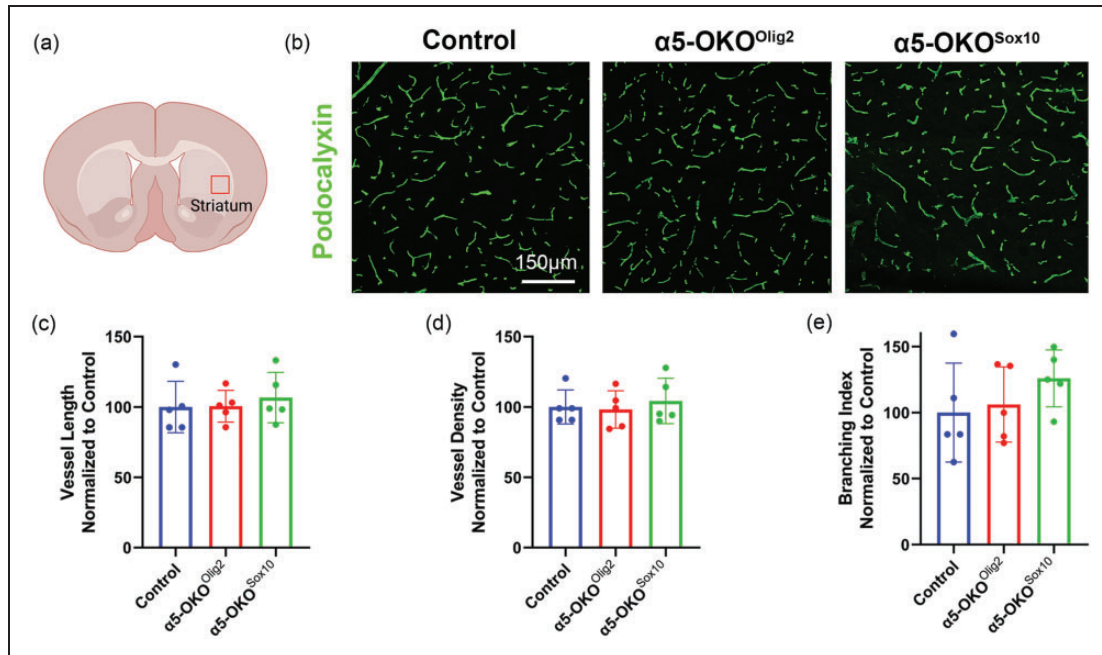**Figure 1.** Loss of OL-derived laminin-α5 does not affect cerebral vasculature under homeostatic conditions. (a) A cartoon indicating the location where images were taken. Created with BioRender.com. (b) Representative images of podocalyxin staining in control, α5-OKO^{Olig2}, and α5-OKO^{Sox10} mice under homeostatic conditions. Scale bar: 150 μm. (c–e) Quantifications of vessel length (c), vessel density (d), and branching index and (e) in control, α5-OKO^{Olig2}, and α5-OKO^{Sox10} mice under homeostatic conditions. n = 5.
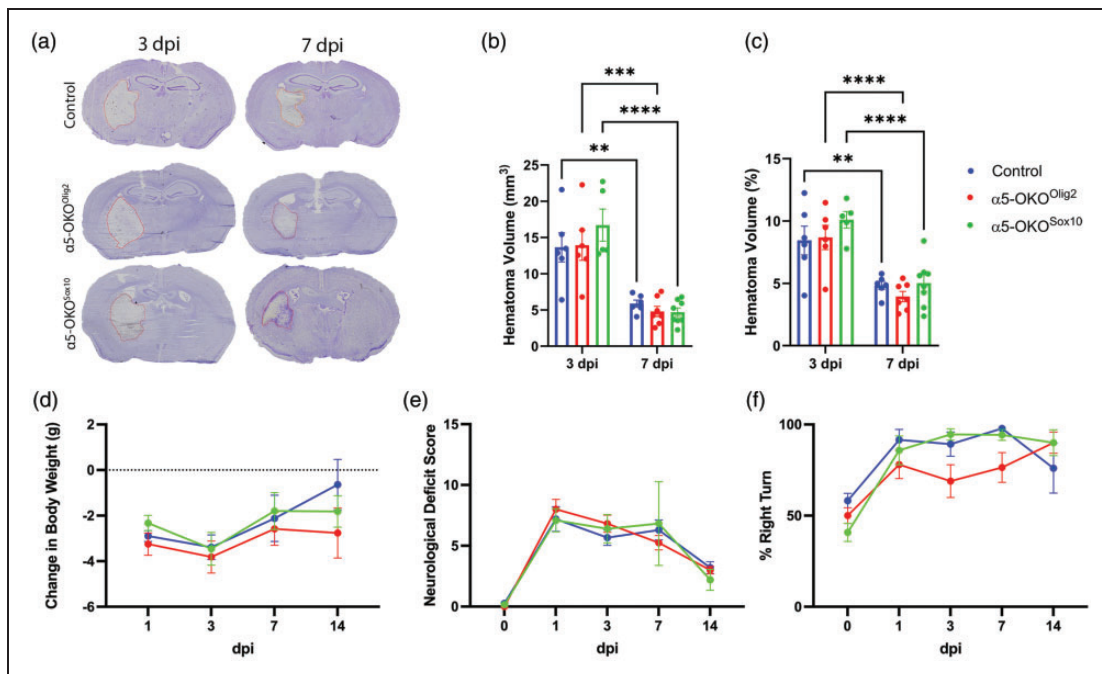
Figure 2. Loss of OL-derived laminin-α5 does not affect ICH outcomes. (a) Representative images of cresyl-violet staining in control, α5-OKO^{Olig2}, and α5-OKO^{Sox10} brains at 3 dpi and 7 dpi. Red lines indicate hematoma area. (b and c) Quantifications of hematoma volume in mm^3 (b) and % (c) in control, α5-OKO^{Olig2}, and α5-OKO^{Sox10} mice at 3 dpi (n = 5–6) and 7 dpi (n = 6–8). (d) Quantification of body weight changes in control, α5-OKO^{Olig2}, and α5-OKO^{Sox10} mice at 1–14 dpi. n = 10–26 for 1–7 dpi and n = 5 for 14 dpi. (e) Modified neurological deficit score in control, α5-OKO^{Olig2}, and α5-OKO^{Sox10} mice at 0–14 dpi. n = 10–24 for 0–7 dpi and n = 5 for 14 dpi and (f) Percentage of ipsilateral turns in control, α5-OKO^{Olig2}, and α5-OKO^{Sox10} mice at 0–14 dpi. n = 7–21 for 0–7 dpi and n = 4–5 for 14 dpi. Data are shown as mean ± SD.

BBB permeability is unchanged in α5-OKO^{Olig2} and α5-OKO^{Sox10} mice

BBB disruption, a key feature of ICH, correlates with ICH outcomes.[3,6] To determine whether loss of OL-derived laminin-α5 affects BBB integrity after ICH, we performed in vivo BBB permeability assay. In sham-operated animals, no hemoglobin signal was detected irrespective of the genotype (Figure 3(a) to (d)). Consistent with this data, negligible levels of IgG were observed in the control and mutant brains (Figure 3(e) to (g)), indicating that loss of OL-derived laminin-α5 does not affect BBB integrity under homeostatic conditions. After ICH, however, strong hemoglobin (Figure 3(b)) and IgG (Figure 3(e)) signals were found in control, α5-OKO^{Olig2}, and α5-OKO^{Sox10} brains, indicating successful induction of ICH. Comparison among genotypes, however, revealed no statistical significance in hemoglobin/IgG intensity and area at either 3 dpi or 7 dpi (Figure 3(c), (d), (f) and (g)). These findings highlight a minimal role of OL-derived laminin-α5 in BBB regulation after ICH. To determine any sex-specific effects, we further analyzed BBB leakage in male and female mice separately. Comparable hemoglobin and IgG levels were found among genotypes at each time point in both sexes (Figure S3). Together, these results suggest a dispensable role of OL-derived laminin-α5 in BBB integrity.

Tight junction protein expression is unaffected in α5-OKO^{Olig2} and α5-OKO^{Sox10} mice

BBB disruption may be caused by increased paracellular transport and/or transcellular transport. Paracellular barrier is maintained by the expression of tight junction proteins, which seal gaps between adjacent endothelial cells.[32–34] Here, we examined the expression of claudin-5 and ZO-1, two tight junction proteins, in the peri-hematoma regions (Figure 4(a)). In sham-operated animals, control mice and both mutant lines (α5-OKO^{Olig2} and α5-OKO^{Sox10}) showed comparable claudin-5 coverage and contact (Figure 4(b), (e) and (f)). Both claudin-5 coverage and contact decreased substantially in all three genotypes at 3 dpi (Figure 4(c), (e) and (f)) and recovered by 7 dpi (Figure 4(d) to (f)), again indicating successful induction of ICH. Comparison among genotypes, however, revealed no statistical significance in claudin-5 coverage or contact at both time points (Figure 4(e) and (f)). Similar to claudin-5, ZO-1 coverage and contact demonstrated comparable changes among genotypes both before and after ICH (Figure S4). These findings suggest that OL-derived laminin-α5 does not regulate tight junction protein expression or paracellular transport.

Caveolin-1 expression is unchanged in α5-OKO^{Olig2} and α5-OKO^{Sox10} mice

Transcellular barrier is maintained by low level of transcytosis in endothelial cells.[35–38] Here, we examined the expression of caveolin-1, a key protein necessary for transcytosis in brain endothelial cells,[39–41] in the peri-hematoma regions (Figure 5(a)). In sham-operated animals, control mice and both mutant lines (α5-OKO^{Olig2} and α5-OKO^{Sox10}) displayed similar caveolin-1 coverage, contact, and intensity (Figure 5 (b) and 5(e) to (g)). Similarly, comparable caveolin-1 levels were detected in control, α5-OKO^{Olig2}, and α5-OKO^{Sox10} mice at both 3 dpi and 7 dpi (Figure 5 (c) to (g)). These results suggest that OL-derived laminin-α5 does not regulate caveolin-1 expression or caveolae-mediated transcytosis.

OL number is unaltered in α5-OKO^{Olig2} and α5-OKO^{Sox10} mice

To investigate if loss of OL-derived laminin-α5 changes their number or proliferation, we performed immunohistochemistry against Olig2 and Ki67 (Figure 6(a) to (d)). Quantification of Olig2$^+$ cells revealed similar numbers in control, α5-OKO^{Olig2}, and α5-OKO^{Sox10} mice in sham group (Figure 6(b) and (e)). Subsequent studies showed that the percentages of proliferating OLs (Olig2$^+$Ki67$^+$ cells) remained the same in control, α5-OKO^{Olig2}, and α5-OKO^{Sox10} mice in sham group (Figure 6(b) and (f)). These results suggest that OL-derived laminin-α5 may not regulate their number and proliferation under homeostatic conditions. Interestingly, comparable OL numbers and proliferation rates were observed in control, α5-OKO^{Olig2}, and α5-OKO^{Sox10} mice at both 3 dpi and 7 dpi (Figure 6(c) to (f)), highlighting a dispensable role of OL-derived laminin-α5 in OL number and proliferation after ICH.

Myelination is unaffected in α5-OKO^{Olig2} and α5-OKO^{Sox10} mice

One major function of OLs is myelination, which is involved in white matter injury/repair. To determine if loss of OL-derived laminin-α5 affects myelination, we analyzed the expression of myelin basic protein (MBP) and myelin-associated glycoprotein (MAG), two major myelin components, along with SMI-32, a marker for demyelinated/damaged axons,[9,42] in the peri-hematoma regions (Figure 7(a)). Compared to the controls, neither α5-OKO^{Olig2} nor α5-OKO^{Sox10} mice showed significant changes in MBP and MAG expression under homeostatic conditions (Figure 7(b), (e) and (f)). No SMI-32 signal was detected in
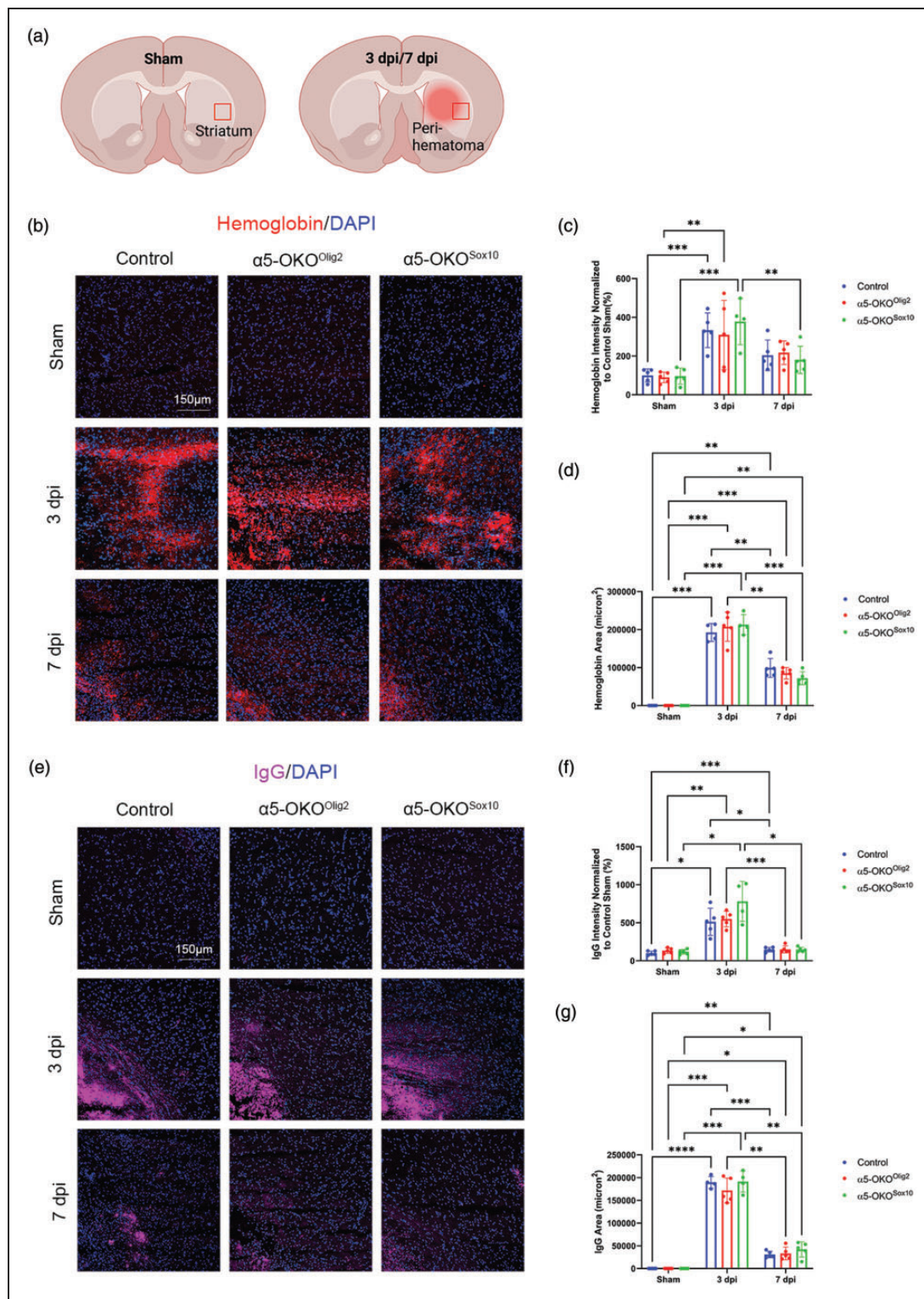
Figure 3. Loss of OL-derived laminin-α5 does not affect BBB permeability. (a) A cartoon indicating the location where images were taken. Created with BioRender.com. (b) Representative images of hemoglobin (red) and DAPI (blue) staining in control, α5-OKO^{Olig2}, and α5-OKO^{Sox10} mice from sham, 3 dpi, and 7 dpi groups. Scale bar: 150 μm. (c and d) Quantifications of hemoglobin intensity (c) and area (d) from sham, 3 dpi, and 7 dpi groups. n = 4–5. (e) Representative images of IgG (magenta) and DAPI (blue) staining in control, α5-OKO^{Olig2}, and α5-OKO^{Sox10} mice from sham, 3 dpi, and 7 dpi groups. Scale bar: 150 μm. (f and g) Quantifications of IgG intensity (f) and area and (g) from sham, 3 dpi, and 7 dpi groups. n = 4–5. Data are shown as mean ± SD.
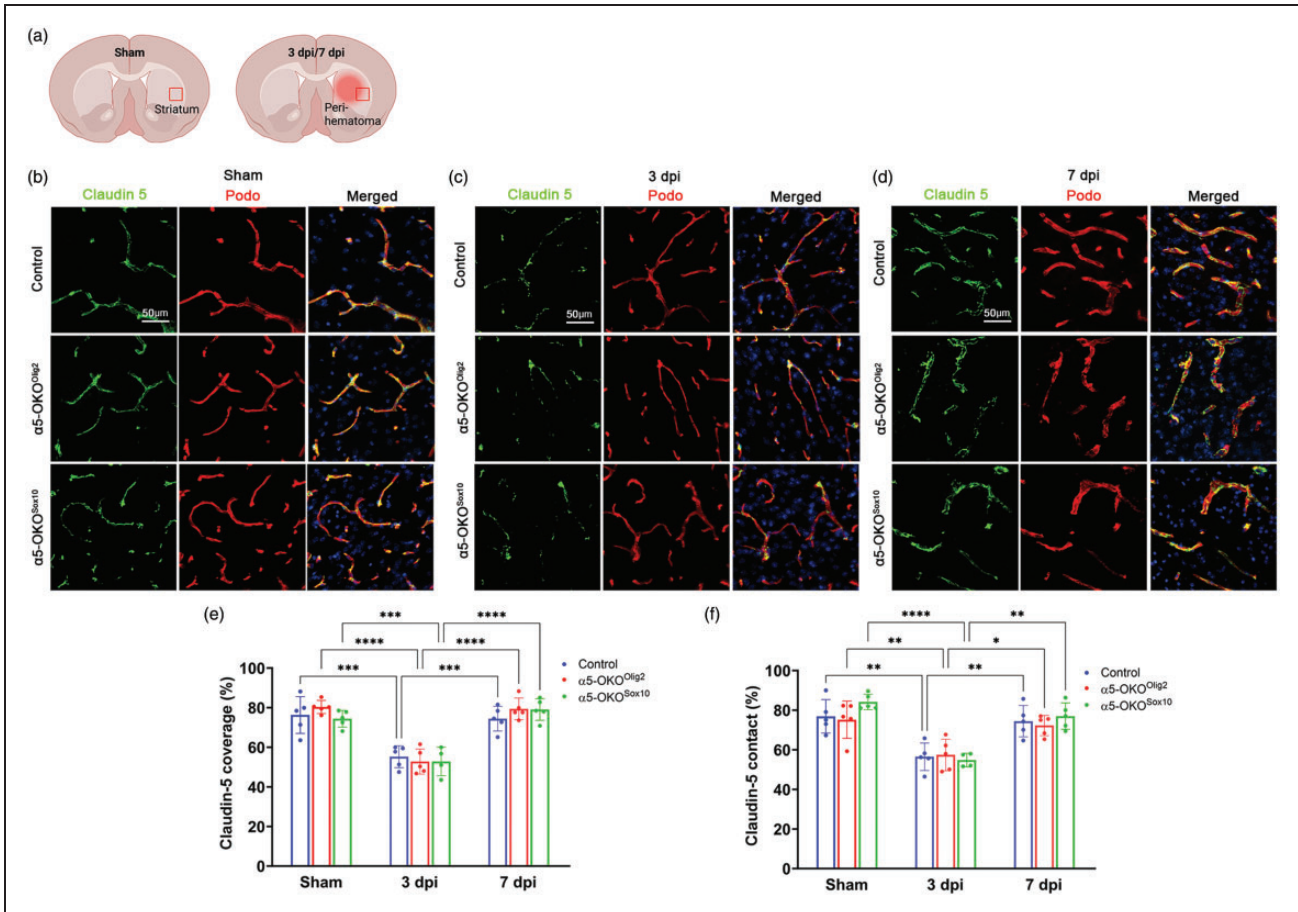
Figure 4. Loss of OL-derived laminin-α5 does not affect claudin-5 expression. (a) A cartoon indicating the location where images were taken. Created with BioRender.com. (b-d) Representative images of claudin-5 (green) and podocalyxin (red) staining in control, α5-OKO^Olig2, and α5-OKO^Sox10 mice from sham (b), 3 dpi (c), and 7 dpi (d) groups. Scale bar: 50 μm. (e and f) Quantifications of claudin-5 coverage (e) and contact (f) in control, α5-OKO^Olig2, and α5-OKO^Sox10 from sham, 3 dpi, and 7 dpi groups. n = 4–5. Data are shown as mean ± SD.

control or mutant brains under homeostatic conditions (Figure 7(b) and (g)). These results suggest a dispensable role of OL-derived laminin-α5 in myelination under homeostatic conditions.

To investigate if OL-derived laminin-α5 participates in white matter injury/repair after ICH,[9,10] we further examined MBP, MAG, and SMI-32 expression in α5-OKO^Olig2 and α5-OKO^Sox10 mice after ICH. Compared to the sham groups, MBP and MAG levels were substantially reduced, while SMI-32 expression was significantly increased after ICH in all genotypes (Figure 7(b) to (g)), again indicating successful induction of ICH. Interestingly, comparisons among genotypes revealed similar MBP, MAG, and SMI-32 levels at both 3 dpi and 7 dpi (Figure 7(e) to (g)). These findings indicate a dispensable role of OL-derived laminin-α5 in myelination or white matter repair after ICH.

Discussion

In this study, we investigated the function of OL-derived laminin-α5 under homeostatic and ICH conditions. First, we confirmed that OL lineage cells express *Lama5* at mRNA level. This is consistent with a previous report showing laminin-α5 expression in pre-OLs.[22] By ablating laminin-α5 expression in OLs using two different Cre lines (Olig2-Cre and Sox10-Cre), we further showed dispensable roles of OL-derived laminin-α5 in brain homeostasis and ICH pathogenesis.

One likely reason for the negative results is that loss of OL-derived laminin-α5 may be compensated by other laminin isoforms synthesized by OLs. There is evidence showing that OLs express various laminin subunits, including laminin-α4 and -α5, at both mRNA and protein levels.[19–22] It is possible that loss of OL-derived laminin-α5 is compensated by
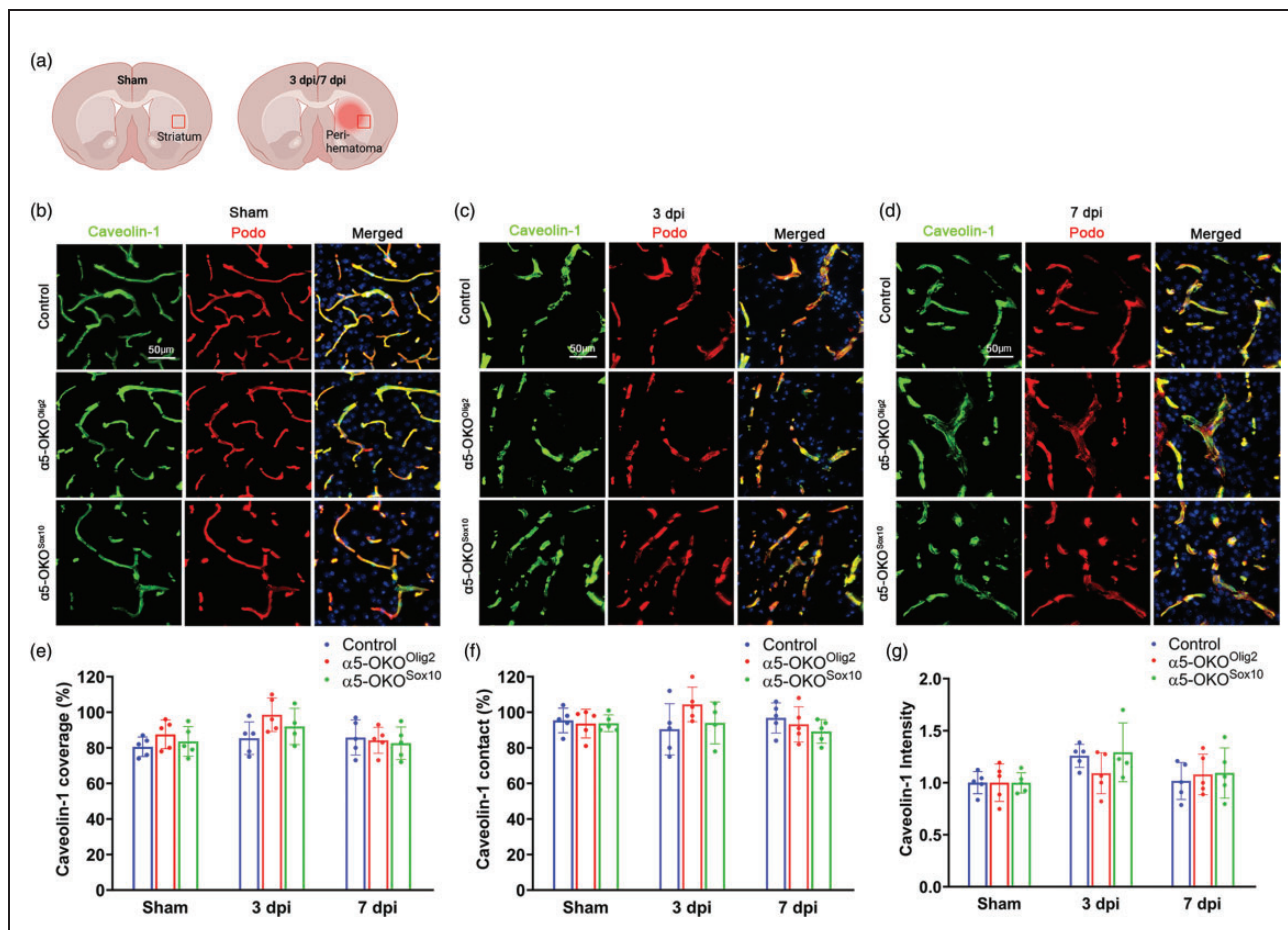
Figure 5. Loss of OL-derived laminin-α5 does not affect caveolin-1 expression. (a) A cartoon indicating the location where images were taken. Created with BioRender.com. (b-d) Representative images of caveolin-1 (green) and podocalyxin (red) staining in control, α5-OKO[Olig2], and α5-OKO[Sox10] mice from sham (b), 3 dpi (c), and 7 dpi (d) groups. Scale bar: 50 μm. (e-g) Quantifications of caveolin-1 coverage (e), contact (f), and intensity (g) in control, α5-OKO[Olig2], and α5-OKO[Sox10] from sham, 3 dpi, and 7 dpi groups. n = 4–5. Data are shown as mean ± SD.

OL-derived laminin-α4. The compensation between laminin-α4 and -α5 has also been found in endothelial cells and mural cells. Specifically, abrogation of endothelial laminin-α5 fails to affect BBB integrity or induce gross abnormalities[15] and laminin-α4 null mice are grossly normal in adulthood,[43] whereas loss of laminin-γ1, which ablates laminin-α4 and -α5 simultaneously, in endothelial cells leads to BBB disruption (unpublished data). Similarly, mice with laminin-α5 deficiency in mural cells are grossly normal and fail to show obvious defects.[16] However, mice with laminin-γ1 deficiency in mural cells, which lack both laminin-α4 and -α5,[13] develop age-dependent BBB breakdown under homeostatic conditions[13] and exhibit aggravated brain injury in an ICH model.[44] Consistent with these findings, our unpublished data demonstrated that deletion of laminin-γ1 in OLs led to BBB compromise, abnormal proliferation and differentiation of OLs, and myelination deficits.

Another possibility is that other cell-derived laminin-α5 may compensate for the loss of OL-derived laminin-α5. Recent single-cell RNAseq studies revealed strong *Lama5* expression in endothelial cells, mural cells, and possibly neurons.[19–21] Consistent with these reports, we and others have shown that endothelial cells,[15] pericytes,[13] and neurons[45] are all able to synthesize laminin-α5 at the protein level. These α5-containing laminin isoforms may take over the function of OL-derived laminin-α5 upon its deletion. Similar compensation has also been observed between endothelial and mural cells. Mice with laminin-α5 deficiency in endothelial cells[15] or mural cells[16] have intact BBB integrity, whereas deletion of laminin-α5 in endothelial and mural cells simultaneously leads to BBB disruption (unpublished data). Future studies should dissect out the potential compensation among different laminin isoforms, which will enable a thorough understanding of laminin's functions.
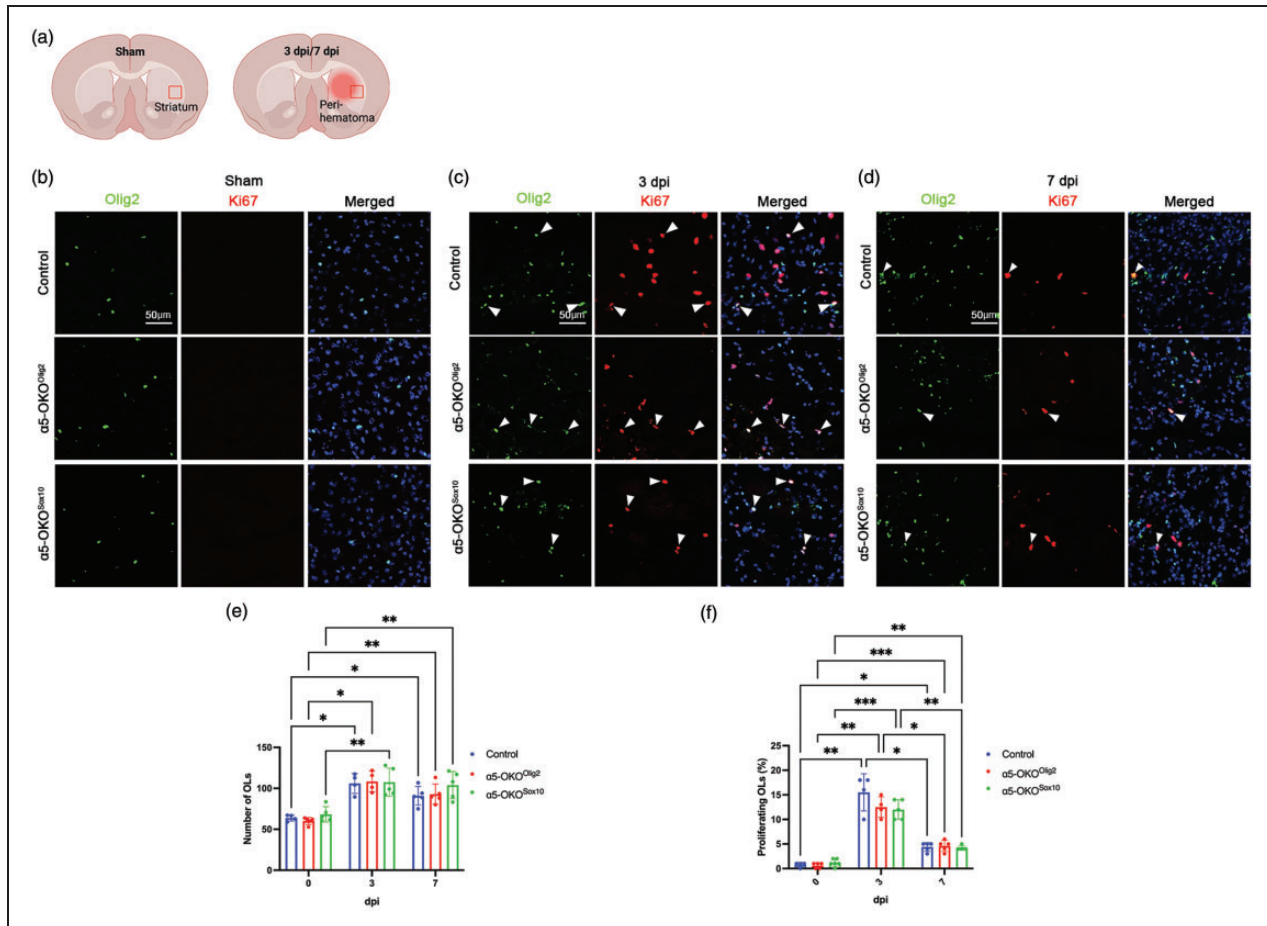
Figure 6. Loss of OL-derived laminin-α5 does not affect OL number and proliferation. (a) A cartoon indicating the location where images were taken. Created with BioRender.com. (b-d) Representative images of Olig2 (green) and Ki67 (red) staining in control, α5-OKO[Olig2], and α5-OKO[Sox10] mice from sham (b), 3 dpi (c), and 7 dpi (d) groups. Scale bar: 50 μm. (e) Quantification of the number of OLs (in 20x images) in control, α5-OKO[Olig2], and α5-OKO[Sox10] from sham, 3 dpi, and 7 dpi groups. n = 4–5. Data are shown as mean ± SD and (f) Quantification of the percentage of proliferating OLs in control, α5-OKO[Olig2], and α5-OKO[Sox10] from sham, 3 dpi, and 7 dpi groups. n = 4–6. Data are shown as mean ± SD.

In this study, both Olig2-Cre and Sox10-Cre lines were used to ablate laminin-α5 expression in OLs. The reason is that, although both Olig2 and Sox10 are used as OL lineage cell markers, neither is specific for OLs.[46] For example, Olig2-Cre also marks some motor neurons[47] and astrocyte precursors,[48] in addition to OL lineage cells.[49–51] Although Sox10-Cre specifically labels OL lineage cells in the CNS,[19,52,53] it also targets other cells in the peripheral, such as Schwann cells.[54,55] Including two conditional knockout mouse lines would allow us to truly investigate the function of OL-derived laminin-α5, since these mutants may share common phenotypes if they are caused by the loss of OL-derived laminin-α5. Surprisingly, these knockout mice and the controls exhibited comparable changes under both physiological and ICH conditions, indicating that OL-derived laminin-α5 is likely dispensable for brain homeostasis and ICH pathogenesis.

One limitation of this study is that only two behavioral tests (neurological severity score and corner test) were performed. It is possible that more sensitive tests, such as adhesive removal test and foot fault test, may reveal behavioral defects in the mutants. These experiments will be conducted in future studies. Another limitation of this study is that the specific laminin isoforms ablated in OLs of the mutants have not been identified. Given that many laminin-β and -γ subunits that can form a trimer with laminin-α5 are expressed in OLs,[19–22] we speculate that multiple α5-containing laminin isoforms are deleted in the mutant mice. Identifying these laminin isoforms would enrich our knowledge on laminin compensation. Next, BBB permeability was mainly assessed using endogenous tracers by immunohistochemistry. Measuring the leakage of exogenous tracers in brain lysate will provide more precise quantification of BBB permeability.
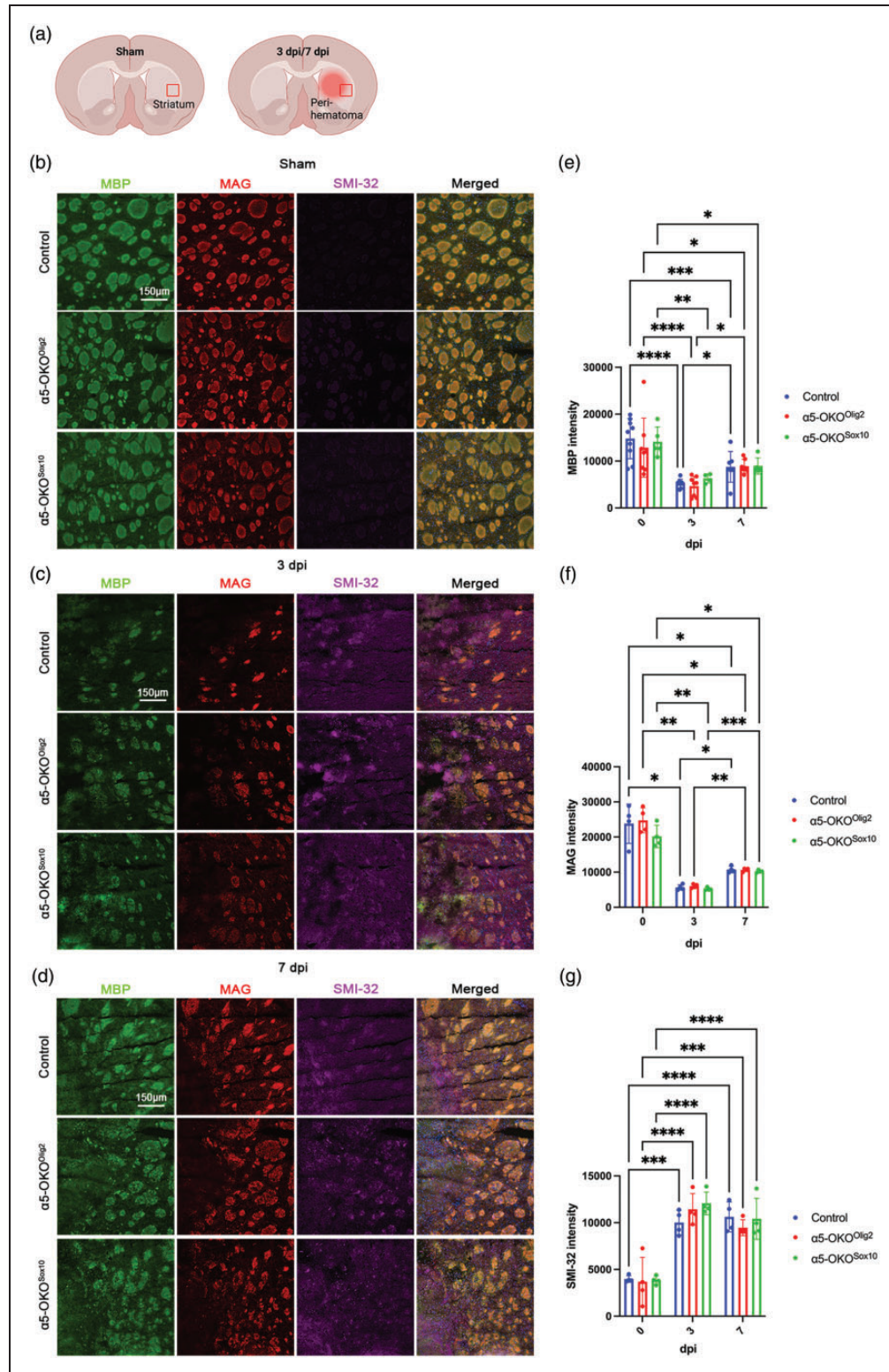
Figure 7. Loss of OL-derived laminin-α5 does not affect myelination and white matter injury/repair. (a) A cartoon indicating the regions of interest where the analyses were done. Created with BioRender.com. (b-d) Representative images of MBP (green), MAG (red), and SMI-32 (magenta) staining in control, α5-OKO^{Olig2}, and α5-OKO^{Sox10} mice in sham (b), 3 dpi (c), and 7 dpi (d). Scale bar: 150 μm. (e–g) Quantifications of the intensities of MBP (e), MAG (f), and SMI-32 (g) in control, α5-OKO^{Olig2}, and α5-OKO^{Sox10} in sham, 3 dpi, and 7 dpi groups. n = 4–9. Data are shown as mean ± SD.

In addition, no in vitro experiments were performed in this study. We will validate major findings using in vitro culture system in the future.

Declaration of conflicting interests

The author(s) declared no potential conflicts of interest with respect to the research, authorship, and/or publication of this article.

Authors' contributions

MK, AN, JR, AA, MG: data acquisition, data analysis, statistical analysis, and manuscript writing; LX: data acquisition and data analysis; YY: conceptualization, experimental design, project supervision, manuscript editing, and funding acquisition. All authors read and approved the manuscript.

ORCID iDs

Jingsong Ruan https://orcid.org/0000-0001-7404-4266
Yao Yao https://orcid.org/0000-0001-8020-9696

Supplementary material

Supplemental material for this article is available online.

References

1. Xu JM, Sherry L, Kochanek Kenneth D, et al. National center for health statistics. (U.S.). Mortality in the United States, 2021. *NCHS Data Brief* 2022; no. 456.
2. Keep RF, Xiang J, Ennis SR, et al. Blood-brain barrier function in intracerebral hemorrhage. *Acta Neurochi Suppl* 2008; 105: 73–77.
3. Keep RF, Zhou N, Xiang J, et al. Vascular disruption and blood-brain barrier dysfunction in intracerebral hemorrhage. *Fluids Barriers CNS* 2014; 11: 18.
4. Ma Q, Huang B, Khatibi N, et al. PDGFR-alpha inhibition preserves blood-brain barrier after intracerebral hemorrhage. *Ann Neurol* 2011; 70: 920–931.
5. Haley MJ and Lawrence CB. The blood-brain barrier after stroke: structural studies and the role of transcytotic vesicles. *J Cereb Blood Flow Metab* 2017; 37: 456–470.
6. Aksoy D, Bammer R, Mlynash M, et al. Magnetic resonance imaging profile of blood-brain barrier injury in patients with acute intracerebral hemorrhage. *J Am Heart Assoc* 2013; 2: e000161.
7. Alvarez-Sabin J, Delgado P, Abilleira S, et al. Temporal profile of matrix metalloproteinases and their inhibitors after spontaneous intracerebral hemorrhage: relationship to clinical and radiological outcome. *Stroke* 2004; 35: 1316–1322.
8. Kang M and Yao Y. Oligodendrocytes in intracerebral hemorrhage. *CNS Neurosci Ther* 2019; 25: 1075–1084.
9. Yao M, Fang J, Li J, et al. Modulation of the proteoglycan receptor PTPsigma promotes white matter integrity and functional recovery after intracerebral hemorrhage stroke in mice. *J Neuroinflammation* 2022; 19: 207.
10. Zheng J, Lu J, Mei S, et al. Ceria nanoparticles ameliorate white matter injury after intracerebral hemorrhage: microglia-astrocyte involvement in remyelination. *J Neuroinflammation* 2021; 18: 43.
11. Kang M and Yao Y. Laminin regulates oligodendrocyte development and myelination. *Glia* 2022; 70: 414–429.
12. Yao Y. Laminin: loss-of-function studies. *Cell Mol Life Sci* 2017; 74: 1095–1115.
13. Gautam J, Cao Y and Yao Y. Pericytic laminin maintains blood-brain barrier integrity in an age-dependent manner. *Transl Stroke Res* 2020; 11: 228–242.
14. Gautam J, Zhang X and Yao Y. The role of pericytic laminin in blood brain barrier integrity maintenance. *Sci Rep* 2016; 6: 36450.
15. Gautam J, Miner JH and Yao Y. Loss of endothelial laminin α5 exacerbates hemorrhagic brain injury. *Transl Stroke Res* 2019; 10: 705–718.
16. Nirwane A, Johnson J, Nguyen B, et al. Mural cell-derived laminin-α5 plays a detrimental role in ischemic stroke. *Acta Neuropathol Commun* 2019; 7: 23.
17. Chen ZL, Yao Y, Norris EH, et al. Ablation of astrocytic laminin impairs vascular smooth muscle cell function and leads to hemorrhagic stroke. *J Cell Biol* 2013; 202: 381–395.
18. Yao Y, Chen ZL, Norris EH, et al. Astrocytic laminin regulates pericyte differentiation and maintains blood brain barrier integrity. *Nat Commun* 2014; 5: 3413.
19. Vanlandewijck M, He L, Mae MA, et al. A molecular atlas of cell types and zonation in the brain vasculature. *Nature* 2018; 554: 475–480.
20. Zhang Y, Chen K, Sloan SA, et al. An RNA-sequencing transcriptome and splicing database of glia, neurons, and vascular cells of the cerebral cortex. *J Neurosci* 2014; 34: 11929–11947.
21. He L, Vanlandewijck M, Mäe MA, et al. Single-cell RNA sequencing of mouse brain and lung vascular and vessel-associated cell types. *Sci Data* 2018; 5: 180160.
22. Kim WK, Kim D, Cui J, et al. Secretome analysis of human oligodendrocytes derived from neural stem cells. *PLoS One* 2014; 9: e84292.
23. Nguyen NM, Kelley DG, Schlueter JA, et al. Epithelial laminin alpha5 is necessary for distal epithelial cell maturation, VEGF production, and alveolization in the developing murine lung. *Dev Biol* 2005; 282: 111–125.

24. Xu L, Nirwane A, Xu T, et al. Fibroblasts repair blood-brain barrier damage and hemorrhagic brain injury via TIMP2. *Cell Rep* 2022; 41: 111709.

25. Shi X, Bai H, Wang J, et al. Behavioral assessment of sensory, motor, emotion, and cognition in rodent models of intracerebral hemorrhage. *Front Neurol* 2021; 12: 667511.

26. Nirwane A and Yao Y. SMAlow/undetectable pericytes differentiate into microglia-and macrophage-like cells in ischemic brain. *Cell Mol Life Sci* 2022; 79: 264.

27. McBride DW, Klebe D, Tang J, et al. Correcting for brain swelling's effects on infarct volume calculation after middle cerebral artery occlusion in rats. *Transl Stroke Res* 2015; 6: 323–338.

28. Zudaire E, Gambardella L, Kurcz C, et al. A computational tool for quantitative analysis of vascular networks. *PloS One* 2011; 6: e27385.

29. Dirnagl U. Bench to bedside: the quest for quality in experimental stroke research. *J Cereb Blood Flow Metab* 2006; 26: 1465–1478.

30. Fisher M, Feuerstein G, Howells DW, STAIR Group, et al. Update of the stroke therapy academic industry roundtable preclinical recommendations. *Stroke* 2009; 40: 2244–2250.

31. Macleod MR, Fisher M, O'Collins V, et al. Good laboratory practice: preventing introduction of bias at the bench. *Stroke* 2009; 40: e50-52–e52.

32. Kniesel U and Wolburg H. Tight junctions of the blood-brain barrier. *Cell Mol Neurobiol* 2000; 20: 57–76.

33. Wolburg H and Lippoldt A. Tight junctions of the blood-brain barrier: development, composition and regulation. *Vascul Pharmacol* 2002; 38: 323–337.

34. Bazzoni G and Dejana E. Endothelial cell-to-cell junctions: molecular organization and role in vascular homeostasis. *Physiol Rev* 2004; 84: 869–901.

35. Abbott NJ, Patabendige AA, Dolman DE, et al. Structure and function of the blood-brain barrier. *Neurobiol Dis* 2010; 37: 13–25.

36. Knowland D, Arac A, Sekiguchi KJ, et al. Stepwise recruitment of transcellular and paracellular pathways underlies blood-brain barrier breakdown in stroke. *Neuron* 2014; 82: 603–617.

37. Chow BW and Gu C. The molecular constituents of the blood-brain barrier. *Trends Neurosci* 2015; 38: 598–608.

38. Andreone BJ, Lacoste B and Gu C. Neuronal and vascular interactions. *Annu Rev Neurosci* 2015; 38: 25–46.

39. Andreone BJ, Chow BW, Tata A, et al. Blood-brain barrier permeability is regulated by lipid transport-dependent suppression of caveolae-mediated transcytosis. *Neuron* 2017; 94: 581–594 e585.

40. Ben-Zvi A, Lacoste B, Kur E, et al. Mfsd2a is critical for the formation and function of the blood-brain barrier. *Nature* 2014; 509: 507–511.

41. Sadeghian H, Lacoste B, Qin T, et al. Spreading depolarizations trigger caveolin-1-dependent endothelial transcytosis. *Ann Neurol* 2018; 84: 409–423.

42. Wang J, Xia J, Zhang F, et al. Galectin-1-secreting neural stem cells elicit long-term neuroprotection against ischemic brain injury. *Sci Rep* 2015; 5: 9621.

43. Thyboll J, Kortesmaa J, Cao R, et al. Deletion of the laminin alpha4 chain leads to impaired microvessel maturation. *Mol Cell Biol* 2002; 22: 1194–1202.

44. Gautam J, Xu L, Nirwane A, et al. Loss of mural cell-derived laminin aggravates hemorrhagic brain injury. *J Neuroinflammation* 2020; 17: 103.

45. Omar MH, Kerrisk Campbell M, Xiao X, et al. CNS neurons deposit laminin α5 to stabilize synapses. *Cell Rep* 2017; 21: 1281–1292.

46. Sock E and Wegner M. Using the lineage determinants Olig2 and Sox10 to explore transcriptional regulation of oligodendrocyte development. *Dev Neurobiol* 2021; 81: 892–901.

47. Lee SK, Lee B, Ruiz EC, et al. Olig2 and Ngn2 function in opposition to modulate gene expression in motor neuron progenitor cells. *Genes Dev* 2005; 19: 282–294.

48. Cai J, Chen Y, Cai WH, et al. A crucial role for Olig2 in white matter astrocyte development. *Development* 2007; 134: 1887–1899.

49. Lu QR, Yuk D, Alberta JA, et al. Sonic hedgehog–regulated oligodendrocyte lineage genes encoding bHLH proteins in the mammalian Central nervous system. *Neuron* 2000; 25: 317–329.

50. Zhang K, Chen S, Yang Q, et al. The oligodendrocyte transcription factor 2 OLIG2 regulates transcriptional repression during myelinogenesis in rodents. *Nat Commun* 2022; 13: 1423.

51. Küspert M, Hammer A, Bösl MR, et al. Olig2 regulates Sox10 expression in oligodendrocyte precursors through an evolutionary conserved distal enhancer. *Nucleic Acids Res* 2011; 39: 1280–1293.

52. Zhang S, Rasai A, Wang Y, et al. The stem cell factor Sox2 is a positive timer of oligodendrocyte development in the postnatal murine spinal cord. *Mol Neurobiol* 2018; 55: 9001–9015.

53. Zhang S, Kim B, Zhu X, et al. Glial type specific regulation of CNS angiogenesis by HIFalpha-activated different signaling pathways. *Nat Commun* 2020; 11: 2027.

54. Reiprich S, Kriesch J, Schreiner S, et al. Activation of Krox20 gene expression by Sox10 in myelinating schwann cells. *J Neurochem* 2010; 112: 744–754.

55. Pingault V, Zerad L, Bertani-Torres W, et al. SOX10: 20 years of phenotypic plurality and current understanding of its developmental function. *J Med Genet* 2022; 59: 105–114.